Bulletin of the Seismological Society of America, Vol. 107, No. 1, pp. –, February 2017, doi: 10.1785/0120160074

Seismic Hazard for Cuba: A New Approach

by Leonardo Alvarez,* Conrad Lindholm, and Madelín Villalón

Abstract A new seismic hazard study for Cuba is presented in terms of maps and uniform hazard spectra (UHS). An earthquake catalog from 1502 to 2012 was prepared for the region 16°–24° N and 67°–86° W, and was homogenized to M_w and cleaned for aftershocks and foreshocks. A 16-arm logic-tree computation corresponding to four source branches and four ground-motion prediction equations (GMPEs) was conducted (using only published GMPE relations due to a lack of local strong-motion data). For each source model, the seismicity parameters (β, λ, and M_{max}) were developed. The results were obtained and are presented in terms of maps and UHS graphs for a 475-year return period, but results for other return periods are easily obtained. The influence of different branch weighting in the logic tree was investigated with respect to the final results. Peak ground acceleration values for Cuba were found to vary from less than 75 to 230 cm/s^2.

Introduction

The seismic history in the Greater Antilles began with the foundation of the first Spanish settlements at the beginning of the sixteenth century. The first Cuban earthquake dates from 1528 (I_{MAX} = VI) in the town of Baracoa (northeastern Cuba), later major ones are associated with Santiago de Cuba in southeastern Cuba (1578 [I_{MAX} = VIII], 1766 [I_{MAX} = IX], 1852 [I_{MAX} = IX], and 1932 [I_{MAX} = VIII], intensities in Medvedev–Sponheuer–Karnik [MSK] scale). Present day seismicity is characterized by high activity in the southeastern part and lower activity in the remaining part of the territory. The first probabilistic estimates of seismic hazard for the Cuban territory were derived by Rubio (1985), and later Alvarez and Bune (1985a) assessed seismic hazard in eastern Cuba using a specially prepared algorithm (Alvarez and Bune, 1985b). These studies were done in terms of macroseismic intensity (MSK). For the present Cuban building code, Chuy and Alvarez (1995) presented a map that shows the horizontal peak ground acceleration (PGA) calculated through a macroseismic intensity—PGA relationship. Later, Rodríguez *et al.* (1997) also calculated the hazard for Cuba, in terms of macroseismic intensity translated into PGA. The first attempts to calculate seismic hazard directly in terms of PGA were done by García *et al.* (2003), also including a logic-tree framework. After that, Garcia *et al.* (2008) used a zoning-free method to develop more hazard estimates for Cuba. García (2007) updated the estimates done in 2003, but he did not include the zonation-free results in the logic tree. The objective of the present work is to obtain new estimates of seismic hazard for Cuba in terms of uniform hazard spectra (UHS). It has to be noted that for the first time the zonation-free method of Woo (1996) is applied to the Cuban region.

Tectonic Setting

Cuba is located on the southern border of the North American plate. The southern part of Cuba borders the Caribbean plate with influence from the major structures surrounding the northern Caribbean. Because of the accumulated understanding of tectonics, seismicity, and recent Global Positioning System measurements of relative displacements (DeMetz *et al.*, 2000; DeMetz and Wiggins-Grandison, 2007; Benford *et al.*, 2012), there is, at present, a common understanding that at the border of the North American and Caribbean plates there are several interacting microplates from the Cayman Islands to the Virgin Islands. Specifically, the southern Cuban margin is in contact with the Gonave microplate (Rosencrantz and Mann, 1991). In Figure 1, a regional deformation model from Benford *et al.* (2012) is presented, in which five of these microplates are indicated.

The Gonave microplate is bounded by the Cayman spreading center to the west, the Oriente fault zone to the north, a system of faults to the south, and the central Hispaniola Mountains to the east. The Oriente fault is a left-lateral transform fault that dominates the seismic activity south of the Cuban mainland. According to Calais and de Lépinay (1991), it has a discontinuous trace characterized by an alternation of sectors with different tectonic characteristics (pull apart basin, strike slip, opening of a deep through and a deformed belt). The Oriente fault delineates the deep trench that can be subdivided into five segments as shown in Figure 2. The type of seismic deformation translates from

*Now at Instituto Nicaragüense de Estudios Territoriales (INETER), Frente al Hospital Solidadridad, Managua, Nicaragua.

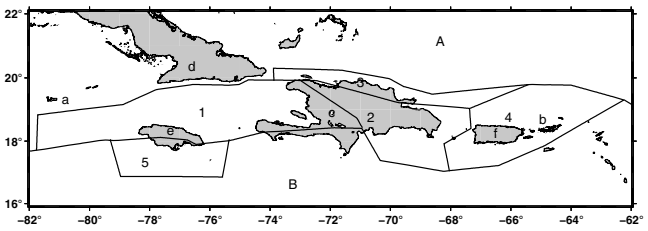

Figure 1. Microplates at the North American–Caribbean plates boundary. (1) Gonave, (2) Hispaniola, (3) Septentrional, (4) Puerto Rico–Virgin Islands, and (5) Jamaica. Geographic features: (a) Cayman Islands, (b) Virgin Islands, (c) Hispaniola, (d) Cuba, (e) Jamaica, and (f) Puerto Rico. (A) North American plate and (B) Caribbean plate. Modified from Benford *et al.* (2012).

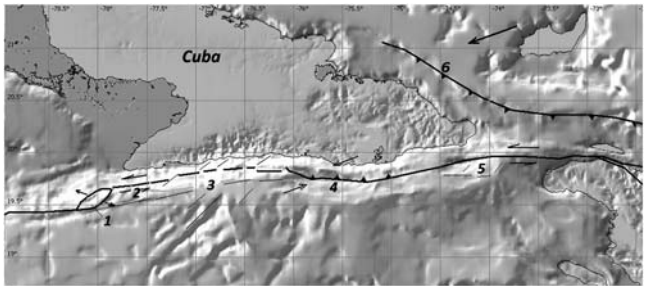

Figure 2. The Oriente fault zone complexity. (1) Cabo Cruz basin (transtension), (2) pure strike slip, (3) opening of the Oriente trough, (4) Santiago de Cuba deformed belt (transpresion), (5) San Nicolás basin (possible transtension), and (6) extension to the northwest of the fault limiting the Septentrional microplate. Modified from Arango (1996).

reverse and transpression in the east toward more strike slip and transtension in the west.

The Cabo Cruz basin is very active with pronounced shallow seismicity and is dominated by normal faults with minor strike-slip components. The Santiago deformed belt is also a very active tectonic structure and is the locus of major earthquakes that have affected Cuba in the past.

The region where the Septentrional fault meets with the Oriente fault is characterized by relatively low seismic activity. This fact raises the question if this seismically quiet segment is really aseismic or if large transpressional earthquakes are expected to rupture this segment after long periods of silence (silence periods exceeding our catalog span).

The geotectonic model of Cuba proposed by Iturralde-Vinent (1998; Fig. 3a) recognized two main levels in the geological structure of Cuba: (1) the fold belt and (2) the Neoautochthon. The fold belt encompasses elements detached from several old tectonic plates (North American, Caribbean, and probably Pacific), whereas the Neoautochthon evolved entirely on a passive segment of the North American plate margin, after the accretionary process that leads to the formation of the fold belt (Iturralde-Vinent, 1996, 1998). At present, there are not enough data to determine the real seismogenetic potential of the faults, which have been mapped by different authors, for example, the map presented in Figure 3b.

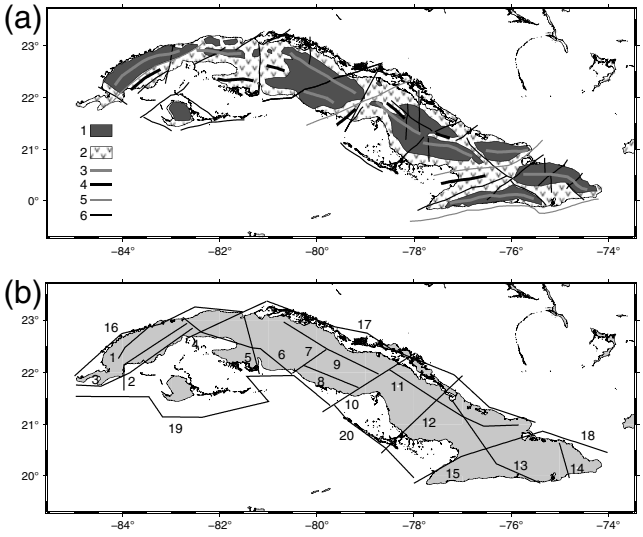

Figure 3. The geology and tectonics of Cuba. (a) Geological model with main fault systems (modified from Iturralde-Vinent, 1998); 1, outcrops of the fold belt; 2, latest Eocene to recent Neoautochthonous deposits; 3, axis of uplift; 4, axis of subsidence; 5, strike-slip faults; 6, normal faults; (b) axes of seismogenetic zones and maximum magnitude estimates (magnitude ranges) for 20 zones within and offshore Cuba (modified from Cotilla and Alvarez, 1991). For zone 20: $M_{max} \leq 5.0$; for zones 1, 4, 5, 6, 7, 8, 11, 12, 13, 14, and 19: M_{max} [5.0–5.5]; and for zones 2, 3, 9, 10, 15, 16, 17, and 18: M_{max} [5.5–7.0].

Earthquake Catalog

An earthquake catalog that covers the period 1502–1995 was already published by Alvarez *et al.* (1999). After 1995, there was a change in the recording capacity of earthquakes in the region; the modernization of seismic networks in Jamaica, Cuba, and Puerto Rico influenced the data processing and hence the catalogs, greatly increasing the volume of available information. It also improved the determination of seismic moment magnitudes (M_w) and a significant effort has been made in reassessing magnitudes and coordinates of past strong and intermediate magnitude earthquakes. In the present work we have compiled a new regional catalog for the northwestern Caribbean for a period from 1502 until 2012. The main sources we used stem from the U.S. Geological Survey (USGS), National Oceanic and Atmospheric Administration (NOAA), International Seismological Centre (ISC)/Global Earthquake Model (GEM), and the local Cuba (Centro Nacional de Investigaciones Sismológicas), Jamaican, and Puerto Rican networks, but contain in addition many other reporting agencies. We considered for every earthquake report the complete set of parameters (epicentral coordinates, depth, origin time, magnitudes, macroseismic data, errors, etc.). The quality of these parameters varies with time, beginning with the less reliable historical reconstructions of felt earthquakes in the past, and ending with the more reliable computer-determined source parameters from instrumental data from recent networks of seismic stations. The sources of data also include macroseismic data (reports,

papers, etc.), instrumental data from international agencies, and finally relocations of epicenters and reevaluation of magnitudes made by different authors.

The work consisted of collecting all data, including different types of magnitudes. For each earthquake, the coordinates were selected between existing sources following the priority order: (a) local relocations of earthquakes, (b) global relocations of earthquakes, (c) data from local networks if the earthquake occurred in the area of maximum reliability of the network, (d) earthquakes from Geological Service National Earthquake Information Service (GS-NEIS), (e) nonrevised ISC earthquakes, and (g) data from other sources. For earthquakes with magnitudes greater than 5, the preferred cases were relocations of hypocenters and reevaluation of magnitudes contained in the Engdahl–van der Hilst–Buland catalog (Engdahl *et al.*, 1998) and the catalog prepared under the ISC/GEM project (Storchak *et al.*, 2013). In both cases, they used special algorithms and updated Earth models for more reliable determinations. For earthquakes of lesser magnitudes, the main sources were local networks, but in many cases the ISC bulletins give more reliable solutions obtained by combination of data from several networks. Local relocations consist in general of a reanalysis of quality of records and adding data from stations outside the original network that result in better solutions. The selection was made case by case. Magnitudes were included for each earthquake until a maximum of 12 differences was reached (by kind and/or source). The general catalog prepared in that way contains 64,541 earthquake records.

Magnitude Conversions

The historical Cuban earthquake catalog was largely established before 1995 following the Soviet school when it was customary to characterize earthquake size within energy classes (K-number; see e.g., Bormann *et al.*, 2012). Because today this is largely history, the whole catalog has been converted to magnitudes following the relations developed for Cuba to this end.

For the macroseismic data, the determination of magnitude and epicenter location was done through modeling of the isoseismals using simple elliptical geometric models (Alvarez and Chuy, 1985) combined with the attenuation given by Fedotov and Shumilina (1971):

$$M_s = (I + 2.63 \log r + 0.0087 r - 2.5)/1.5 \quad (M > 3). \quad (1)$$

Magnitudes determined by intensity data are termed M_I.

The Cuban local network determined from 1968 to 1997 two variants of magnitudes. The first is the classical energy number Kr of Rautian (Rautian *et al.*, 2007), and the second is a duration magnitude, M_D. A relationship with M_s was derived for the Kr, whereas the M_D was calibrated directly with M_s (Alvarez *et al.*, 1999). The relationships, valid for $M_s < 4.5$, are

Table 1
Distance and Time Windows Determined by Rodríguez and Alvarez (1996) for Aftershocks Removal

Magnitude	L (km)	T (days)
3.5	10	14
4	20	20
4.5	26	28
5	35	38
5.5	40	50
6	48	70
6.5	55	100
7	65	160
7.5	74	170
8	85	180

$$M_s(\mathrm{Kr}) = 0.48\mathrm{Kr} - 1.5,$$
$$M_s(D) \approx M_D = 3.2 \log D - 4.5. \quad (2)$$

As discussed by Alvarez *et al.* (2000), these relations were obtained from a sample of earthquakes for which magnitude M_s, energetic class Kr, and duration D was determined from seismograms independently. Finally, the catalog was homogenized to M_w by a direct conversion of m_b and M_s to M_w following the Scordilis (2006) global relations.

It is necessary to observe that after 1968 there was a technological change in the Cuban network, and new local magnitudes (M_L and M_D or M_c) began to be determined. These magnitudes reflect a big dispersion with respect to m_b or M_s and no conversions to M_w could be determined. The same problem arises with the local Puerto Rican magnitudes that began to appear after 1997. As these local magnitudes cannot be converted to M_w, the earthquakes that only have those magnitudes were excluded from the quantitative analysis of seismicity.

The precision of magnitudes in the final catalog is not uniform. The M_w values in the ISC/GEM catalog have determinations of uncertainty, the majority in the 0.2–0.5 range. The conversions from (m_b, M_s) to M_w using the Scordilis formulas naturally introduce an additional uncertainty due to the dispersion of the relations. The conversion from macroseismic data and local earthquake magnitudes to M_s has an unknown uncertainty and it depends on the available amount of macroseismic data. In the case of local Cuban magnitudes prior to 1998, we do not have uncertainty determinations.

Declustering of Foreshock and Aftershock

The procedure used for eliminating dependent events was the one developed by Gardner and Knopoff (1974), as implemented in the cluster program in the SEISAN software (Ottemöller *et al.*, 2013). In this declustering approach, an event is considered an aftershock if it lies inside a set of time–space–magnitude windows. Rodríguez and Alvarez (1996) obtained the local time–space and time–magnitude windows for Caribbean data that we decided to use (see Table 1).

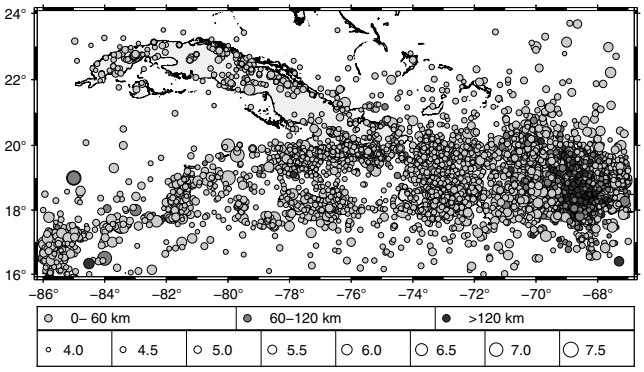

Figure 4. Earthquake epicenters map, final catalog. First line in the legend corresponds to depth and second line to magnitude M_w.

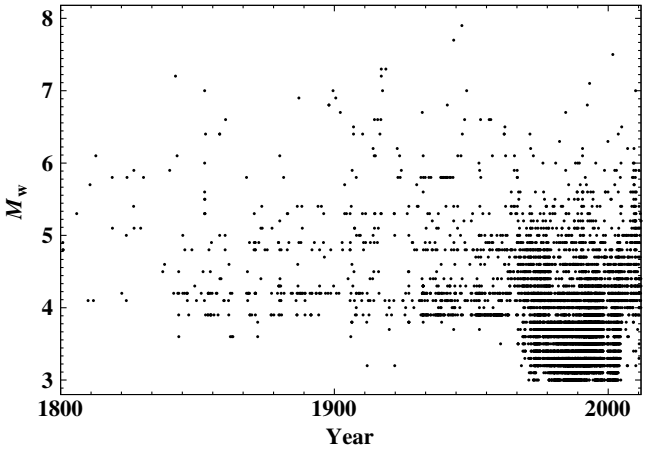

Figure 5. Magnitude–time distribution from 1800, $M_w > 3$.

Following the removal of dependent earthquakes, the regional earthquake catalog was reduced to 13,073 earthquakes with M_w magnitudes, and this catalog was used in the subsequent analysis for the determination of spatial windows and extraction of recurrence parameters. The epicenter map and other information about catalog characteristics are presented in Figures 4 and 5.

Analysis of Completeness

In the current study, we used the principle that the earthquake occurrence should follow a log–linear distribution in the magnitude domain (Stepp, 1972). The earthquake catalog was first divided into several subcatalogs. At the end, two main subcatalogs with different characteristics were identified: (a) the earthquakes covering Cuba and the near surroundings and (b) the earthquakes outside Cuba. The data were used for preparing the cumulative occurrence by time–magnitude intervals as well as tables containing the number of earthquakes inside $(\Delta T, \Delta M)$ intervals. The main attention was given to the $(\Delta T, \Delta M)$ tables, varying both ΔT and ΔM. In Table 2, there is a summarized example of this earthquake occurrence representation.

Table 2
Example of $(\Delta T, \Delta M)$

	Magnitude Intervals of $\Delta M = 0.5$*							
Period	3.5	4.0	4.5	5.0	5.5	6.0	6.5	7.0
1498–1872	0	1	1	0	16	14	***7***	***9***
1873–1902	0	44	11	10	3	1	***0***	***0***
1903–1932	2	34	18	18	***10***	***5***	***1***	***0***
1933–1942	0	77	12	***15***	***4***	***4***	***0***	***0***
1938–1947	1	66	10	***13***	***1***	***5***	***1***	***0***
1948–1957	1	95	8	***14***	***2***	***0***	***0***	***0***
1958–1967	1	96	6	***9***	***1***	***0***	***0***	***0***
1968–1972	48	71	***38***	***5***	***0***	***0***	***0***	***0***
1973–1977	200	***127***	***74***	***10***	***0***	***1***	***0***	***0***
1978–1982	149	***101***	***17***	***4***	***1***	***0***	***0***	***0***
1983–1987	189	***86***	***22***	***2***	***1***	***0***	***0***	***0***

*Each cell gives the number of earthquakes N in the $(\Delta T_i, \Delta M_j)$ interval. Cases are sought, in which by moving horizontally to the left, the Stepp's log-linearity condition is fulfilled. For low magnitudes, short-time intervals are used. For intermediate magnitudes, it is necessary to use larger ΔT intervals and the procedure is the same, whereas for maximum magnitudes in general it is necessary to search the whole time span of the catalog. The identified completeness intervals are shown with bold italic values of $N(\Delta T_i, \Delta M_j)$.

Development of Recurrence Parameters

Let $n(m)$ represent the density of occurrence of earthquakes; then $n(m)dm$ is the quantity of earthquakes in the interval $[M - dM/2$ to $M + dM/2]$ (Utsu, 1971). The general form of the Gutenberg–Richter law is then

$$\begin{array}{ll} n(M) = 10^{a-b(M-M_0)} & M \le M_{\max} \\ n(M) = 0 & M > M_{\max} \end{array}, \tag{3}$$

in which M_0 is an arbitrary reference magnitude.

The computation of earthquakes within each magnitude interval can be written as (N_i, M_i) in which $N_i = N(M_i) = N(M_i - \Delta M/2, M_i + \Delta M/2)$. Integrating $n(M)$ inside the interval we obtain

$$N(M_i) = 10^{a-b(M_i-M_0)} \times \left[10^{\frac{b\Delta\Delta}{2}} - 10^{\frac{-b\Delta M}{2}}\right]/(b \times \ln 10). \tag{4}$$

The value of λ used in the probabilistic approach of seismic hazard is the number of earthquakes in the interval $(M_{\min}, M_{\max})$, that is, $\lambda = N(M_{\min}, M_{\max}) = N_\Sigma(M)|M = M_{\min}$, in which

$$N_\Sigma(M) = \left\{\frac{10^{a-b(M-M_0)}}{b \times \ln 10}\right\} \times [1 - 10^{-b(M_{\max}-M)}]. \tag{5}$$

Through the above formulation, the cumulative double-truncated earthquake recurrence model has been computed (see e.g., Alvarez, 1985).

The procedure for obtaining the parameters β and λ is as follows. The parameters a and b are obtained by linear

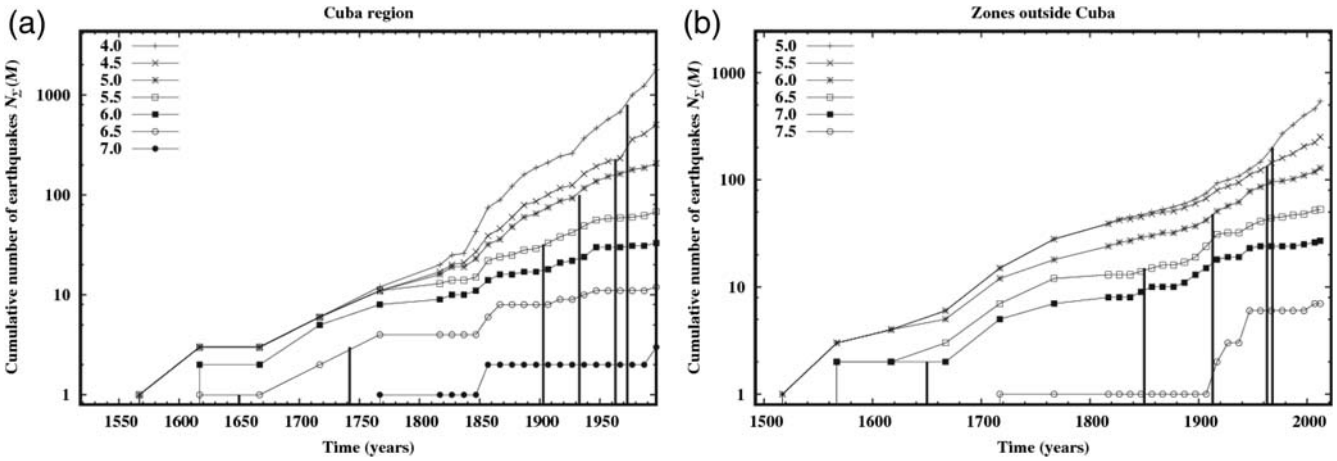

Figure 6. Stepp's graphics for both the major regions considered: (a) Cuba and (b) zones outside Cuba. The value of the central magnitude in each magnitude interval is indicated in the legend. Vertical discontinuous lines mark the beginning of completeness times for each magnitude interval.

regression of formula (4), with $M_0 = 0$, in which the values of $N(M_i)$ are obtained by counting the earthquakes inside the completeness intervals, normalized by the time span. Then, the values of β and λ are obtained as $\beta = b \times \ln(10)$ and λ by evaluating $N_\Sigma(M)|_{M=4.5}$ in formula (5).

Because of the different characteristics of the catalog for Cuba and the remaining part of the study region (Cuban mainland is complete for lower magnitude thresholds), the parameters were calculated separately for these regions (Cuban mainland surrounding regions). The completeness intervals are presented in Table 3, and in Figure 6 the corresponding Stepp's graphics are shown. The regressions were done by three methods (least squares, maximum likelihood, and reduced major axis), with very similar results. The obtained parameters were Cuban mainland and surrounding ($a = 6.37$, $b = 1.18$, $\beta = 2.72$, $\lambda = 3.83$) and remainder zones ($a = 6.26$, $b = 1.04$, $\beta = 2.39$, $\lambda = 14.69$). The correlation coefficients for Cuba were $r = -0.996$ and -0.999 for the other zone.

Table 3
Magnitude Completeness Thresholds Determined for the Cuba Region and for Zones outside Cuba

Cuba Region			Zones outside Cuba		
M_w	$T1$*	$T2$	M_w	$T1$	$T2$
4	1973	1997			
4.5	1963	2002			
5	1933	2012	5	1968	2012
5.5	1903	2012	5.5	1963	2012
6	1903	2012	6	1913	2012
6.5	1742	2012	6.5	1850	2012
7	1650	2012	7	1650	2012
			7.5	1650	2012
			8	1502	2012

*$T1$ is the first year of complete recording and $T2$ is the last. The completeness interval is ($T1$, $T2$); the values of M_w correspond to the center of a magnitude interval of width 0.5. The time $T2$ is less for magnitudes 4 and 4.5 in the Cuba region because of the challenge of magnitude calculations (see the Magnitude Conversions section).

Source Models

We applied a computational probabilistic seismic-hazard analysis (PSHA) method combining three alternative source models: (a) area zonation, (b) fault modeling, and (c) zoning-free model based on a generalized Poissonian seismicity directly derived from the catalog (the Kernel approach proposed by Woo, 1996). The recurrence parameters have been derived from different approaches for the three source models.

The area zonation models were defined with different details from a combination of seismicity distribution and the regional seismotectonics: a coarse 9-zone model (Fig. 7) and a fine 39-zone model (Fig. 8). The coarse model is based only on the main features, whereas the fine model takes into account also the detailed seismotectonic knowledge (Fig. 3) and the earthquake occurrence characteristics.

The recurrence parameters in both cases were defined fitting the seismicity to a Gutenberg–Richter law. The β values were estimated from the larger zones (more stable regressions) and the λ values were estimated individually for both the fine and coarse zonations. The M_{max} values were identified for each zone based on expert opinion and historical seismicity (see also Table 4 and Fig. 3). As a rule of thumb, the M_{max} assigned to the zones were at least five decimals higher than the historical M_{max}.

The fault model (Fig. 9) consisted of 21 quantifying active mapped faults, 19 from the USGS Open-File Report of r97-470 (see Data and Resources) and 2 from Cotilla and Alvarez (1991), of which several were subdivided into smaller segments. The derived activity was divided equally between the line sources and the areas encapsulating the fault out to 25 km distance.

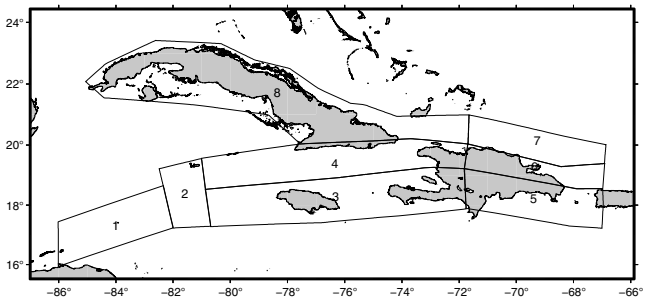

Figure 7. Definition of nine main zones, coarse zones, used in the earthquake quantification process. The numbers correspond to the ones in Table 4. A zone covering the deep Dominican Republic subduction area (number 9 in Table 4) is not shown to avoid picture cluttering. Its spatial limits correspond to the joining of zones 5 and 6.

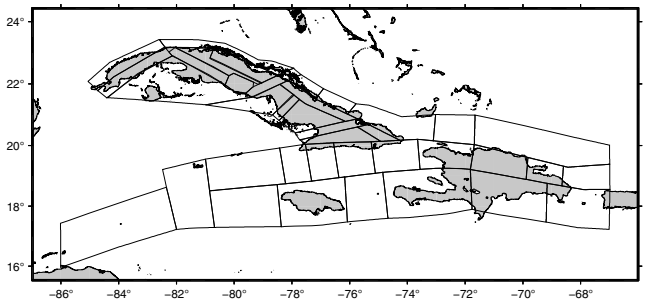

Figure 8. Definition of 39 smaller zones, fine zones, used in the earthquake quantification process. A zone covering the deep northern Dominican Republic subduction area is not shown to avoid picture cluttering.

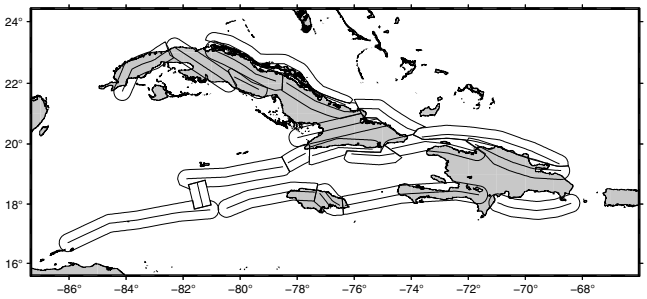

Figure 9. Definition of 21 faults (two merged) used in the earthquake quantification process. Each fault was defined twice; once as a line source and once as an area surrounding the surface fault trace. The faults are considered as the major mapped faults of the region (Cotilla and Alvarez, 1991, U.S. Geological Survey [USGS] Open-File Report of r97-470, see Data and Resources).

The quantification of the fault model was done by simple normalization: counting the events within the zones surrounding the line sources N_{zone}, and multiplying the overall total λ_T value obtained for the region by the fraction $N_{\text{zone}}/N_{\text{region}}$.

The key to the fault model is that it is complementary to the conventional area zones where seismicity is somewhat smeared out. The fault model is complementary because it reflects the geometry of mapped faults suspected to be active, thereby concentrating the activity geographically.

In the case of the non-Poissonian model, we used the zoning-free method Kergrid suggested originally by Woo (1996), where seismicity is described in a grid. Until now it has not been widely used (see also Molina *et al.*, 2001), but recently has gained some interest (Ornthammarath *et al.*, 2008; Crespo *et al.*, 2014; Ashish *et al.*, 2016). The fundamental principle is well known: namely a more direct use of the earthquake catalog rather than using parameterized and simplified recurrence model parameters. The new approach is that each earthquake is treated as a center of a seismic source such that a kernel probability function of occurrence rate is constructed around it. Furthermore, the normal completeness estimate of a catalog (which most often excludes older data from being quantitatively used) is substituted with a magnitude-probability-for-reporting function such that a matrix is constructed for different time windows and time intervals indicate the probability of detectability. With this approach an effective cumulative observability can be established, and the full catalog is used to the maximum of its information value. This represents a significant advantage over traditional quantification dependent on completeness. The Woo (1996) method is furthermore not dependent on the doubly truncated Gutenberg–Richter recurrence, but rather on a generalized Poissonian recurrence, which follows the observed seismicity more closely.

In our case, the grid established consisted of 1800 points spaced 0.2° in latitude and longitude and covering all the Cuban and adjacent regions and using data from the seismic catalog in the magnitude range M_{w} (4.5–7.5) with steps of $\Delta M = 0.5$. For each magnitude range, a table of effective observation period was established so that the full catalog of $M_{\text{w}} \geq 4.5$ could be used.

These models form four main branches of a logic tree. In the following, they will be referred to as coarse (9-zone area model), fine (39-zone area model), faults (fault model), and Kergrid (zoning-free method). For each of the branches, the recurrence parameters were computed.

Table 4
Recurrence Parameters Used for the Hazard Calculation with the Coarse Model

Name of Zone	λ	β	M_{max}
West Cayman	2.95	2.49	7
Cayman	0.842	2.49	6.5
Jamaica	1.99	2.49	7.8
Oriente	3.52	2.49	7.8
South Dominican Republic	2.42	2.49	7.5
Central Dominican Republic	3.79	2.49	8
North Dominican Republic	1.2	2.49	6.8
Cuba	0.89	2.49	6.7
Deep Dominican Republic	3.391	2.45	7.5

Ground-Motion Prediction Equations

The selection of appropriate ground-motion prediction equations (GMPEs) for use in PSHA modeling is a challenge;

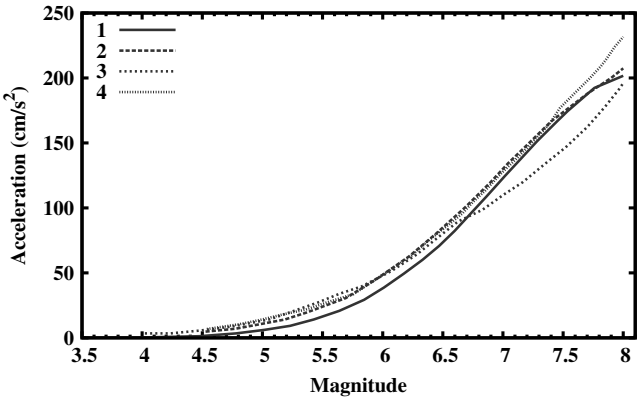

Figure 10. Magnitude-scaling characteristics of the four relations used (scaling example for TUHS = 1 s, epicentral distance = 0 km, and depth = 15 km). 1, Atkinson and Boore (2006); 2, Pezeshk *et al.* (2011); 3, Campbell and Bozorgnia (2008); 4, Abrahamson and Silva (2008).

within Cuba the scarcity of strong-motion data at short distances from historical earthquakes does not allow for good constraints for a new relation. Additionally, in the region we have a stable continental region (SCR) type as well as oceanic crust and active deformation zones to the south where the east–west-trending Oriente fault system constitutes the divide between the North American continent and the Caribbean plate. In this situation where we use multiple models in very different environments, we used the experience and expertise developed by others.

The GEM project (see Data and Resources) had an international expert group evaluating the globally available GMPEs. These expert group recommendations discussed the use of several relations developed for both active and SCR type regions. In the present study, we used a combination of the following GMPEs that were recommended by the GEM expert group (Douglas *et al.*, 2013):

- Campbell and Bozorgnia (2008) for active crust (deformation zones related to the plate boundary),
- Abrahamson and Silva (2008) for active crust (deformation zones related to the plate boundary),
- Pezeshk *et al.* (2011) for stable continental regions (mainly within and around Cuba), and
- Atkinson and Boore (2006) for stable continental regions (mainly within and around Cuba).

These four relations are quite distinct and vary significantly in intensity as well as scaling with distance and magnitude. Figure 10 demonstrates a relative homogeneous magnitude scaling for spectral acceleration SA(1 s).

The chosen relations were used in the logic-tree combinations as shown in Figure 11. For the Kergrid branch, it was not possible to use different GMPEs for different source points, and we decided to use single relations for individual arms.

The Logic Tree

The final computation was conducted in a weighted logic tree where the weighting could be varied. The focal depth

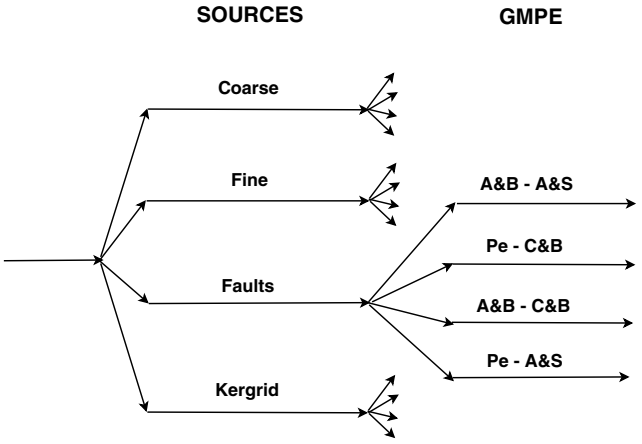

Figure 11. Logic tree with a total of 16 arms formed by four branches with four arms each. The ground-motion prediction equations (GMPEs) are combined with one for the active region and one for the stable continental crust reflecting the source tectonics. Abbreviations in GMPE are: A&B, Atkinson and Boore (2006); A&S, Abrahamson and Silva (2008); Pe, Pezeshk *et al.* (2011), and C&B, Campbell and Bozorgnia (2008). In the case of the Kergrid source model, the characteristics of the method allow the use of more than one GMPE, and the arms correspond to each GMPE alone. Coarse and Fine indicate the two area zonations.

selected (for GMPEs using hypocenter distance or distance to rupture) was 15 km for mainland Cuba. Only results for mainland Cuba were computed. The calculations of seismic hazard were performed with program CRISIS2014 (Ordaz *et al.*, 2014), which is capable of processing together both the classical cases of areas, lines, and points sources with associated Gutenberg–Richter recurrence relations, and zoneless cases with generalized Poissonian occurrence model.

Results

The probabilistic hazard models obtained are described in terms of PGA hazard maps at 10% exceedance probability in 50 years along with spectra for selected cities at the same exceedance probabilities. All results refer to computations at rock outcrop sites (National Earthquake Hazards Reduction Program type B conditions). Additionally, while not shown here, such maps have been obtained for seven other periods of UHS considered in the calculations.

Some of the PGA results for various weighting of the input branches are shown in Figures 12–14 for PGA. Obviously, there is a large family of weighting models that may be acceptable, and we herein only show two differently weighted PGA models. Figure 12 corresponds to equal weighting and Figure 13 corresponds to a half-weighting of coarse and Kergrid branches, whereas in Figure 14 we show the results corresponding to the four individual branches alone. Figure 15 shows six UHS spectra with equal weighted models for very different sites of Cuba: Pinar del Río, La Habana, Santa Clara, Bayamo, Santiago de Cuba, and Guantánamo.

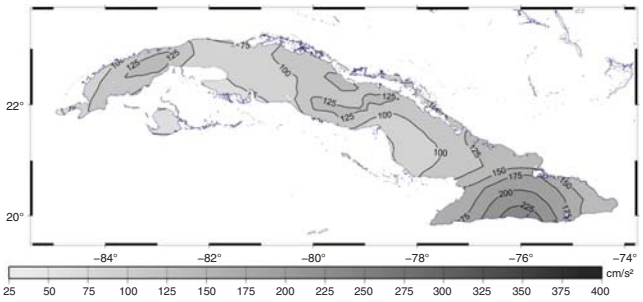

Figure 12. Peak ground acceleration (PGA) hazard for 10% in 50-year exceedance probability (four branches with equal weight, 16 arms). All models weigh equally, $\text{Max}_{\text{PGA}} = 237$ cm/s^2 onshore. The color version of this figure is available only in the electronic edition.

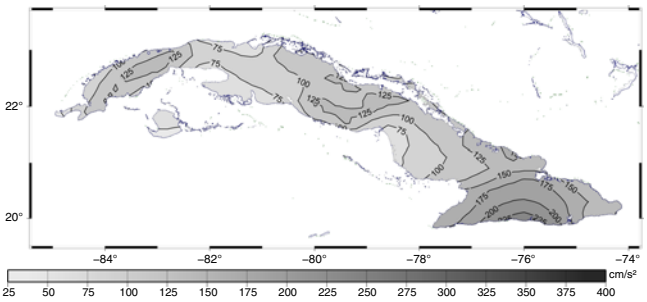

Figure 13. PGA hazard for 10% in 50-year exceedance probability. Half-weight on coarse and Kergrid branches, $\text{Max}_{\text{PGA}} = 230$ cm/s^2. The color version of this figure is available only in the electronic edition.

Discussion and Conclusions

The processing of all this data with the CRISIS2014 software (Ordaz *et al.*, 2014) using the logic-tree approach allowed us to obtain a set of maps and graphics showing different representations of seismic hazard. All computations were conducted for 10% exceedance probability in 50 years (corresponding to a 475-year return period).

The above examples of hazard maps and spectra are only a few examples on how the various combinations of models (branches) may yield different hazard results depending on the weight given to a particular model. It is, for example, obvious how the fault branch leads to a more distinct hazard concentration around the faults, whereas the more truthful Kernel branch reflects past seismicity distribution with very high hazard assigned to southern Cuban coast areas.

We avoided the selection of the best weighting model in the present investigation, because this implicitly reflects the seismotectonic concepts of the individual selector. A pragmatic solution could be to promote in particular the equal weighted solution, however, if doing so, one should recognize that this model also equalizes the concepts behind the four-branched logic-tree model, and this may certainly be challenged.

Earthquake PSHA attempts to include the inherent randomness of earthquake occurrence and the shaking produced from earthquakes at given distances and at given periods. Nevertheless, it depends critically on empirical information (catalogs, reliable magnitudes and locations, and reliable GMPEs), which is the most uncertain basis also for the present hazard computation. The catalog magnitudes, completeness periods, and earthquake locations are all subjected

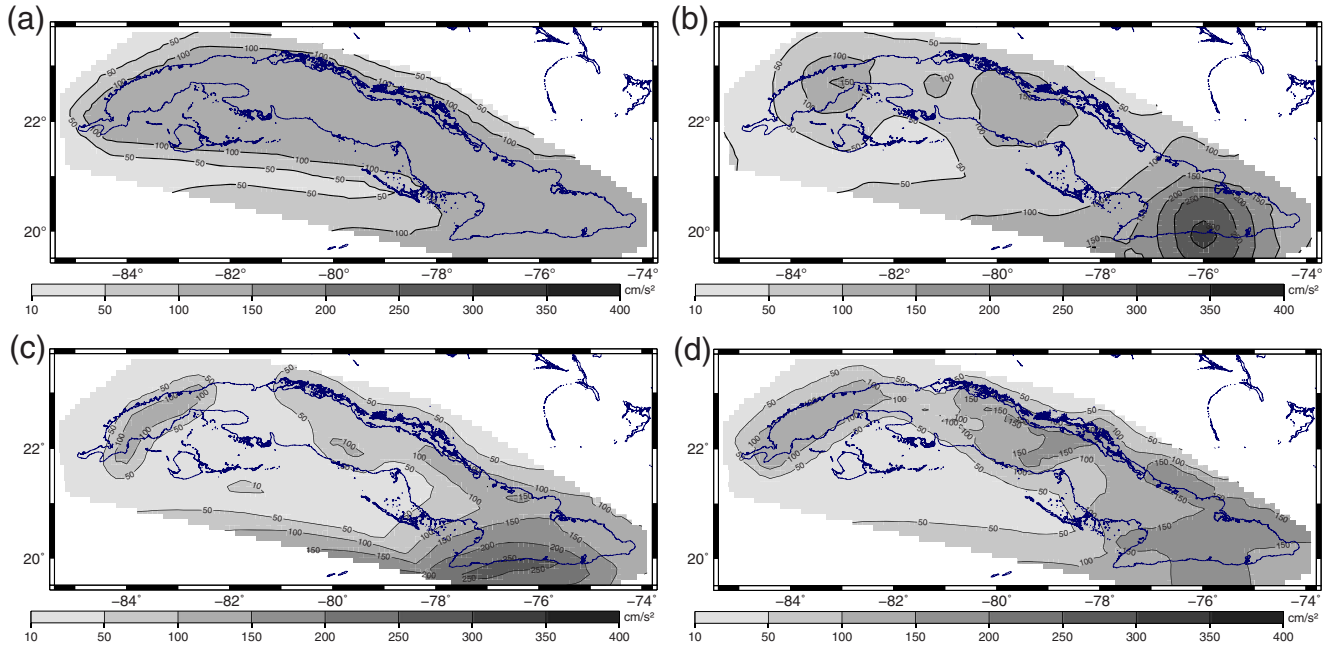

Figure 14. PGA hazard for 10% in 50-year exceedance probability. Individual contribution of all the branches: (a) coarse areal model, (b) Kergrid model, (c) faults model, and (d) fine areal model. The color version of this figure is available only in the electronic edition.

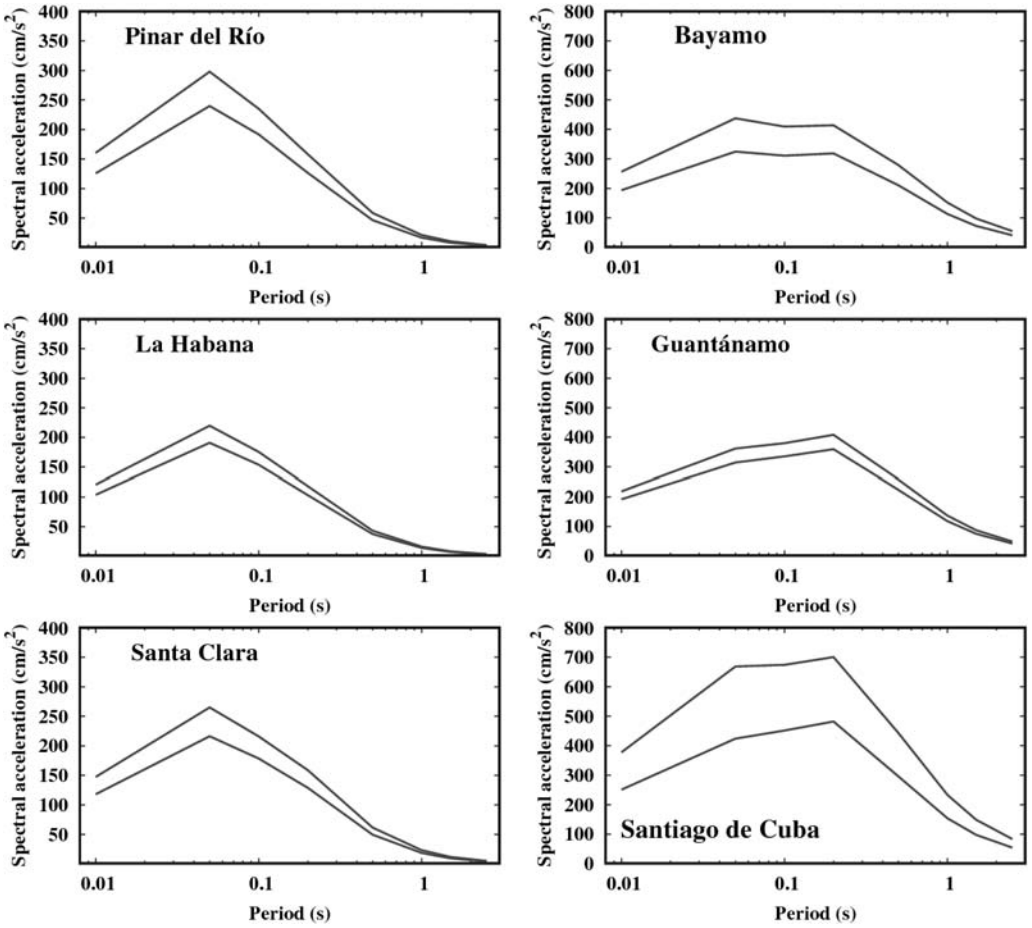

Figure 15. Uniform hazard spectra calculations for six cities in Cuba, three in the western part (Pinar del Río, La Habana, and Santa Clara) and three in the southeastern part (Bayamo, Guantánamo, and Santiago de Cuba). Return period 475 years, all arms equally weighted. In each graphic, the average values over all arms (lower curve) and the average values plus the epistemic uncertainty (upper curve) are represented. The vertical scale is different for western and eastern cities.

to increasing uncertainty when going back in time (and up in magnitude), and likewise the zonation is subjective and the line fault activity only reflects mapped fault structures (blind faults are, for natural reasons, not included). In spite of all the inherent uncertainties, we believe that the obtained results represent a useful step on the ladder toward more reliable hazard estimates, not the least through application of more recent GMPEs.

A comparison with already published results in terms of PGA for a 475-year return period (García, 2007; Garcia *et al.*, 2008) shows that our results for PGA + SDe (SDe is the epistemic standard deviation or σ_e) are comparable with the García (2007) zonified cases for PGA + SDa (SDa is the aleatoric standard deviation) and with some of them presented by Garcia *et al.* (2008) for nonzonified cases. In these works, there has never have been a unification of both kinds of cases in a single logic tree. This is a big difference with our results that makes it difficult to do numerical comparisons.

Another possible comparison, although difficult, is with the seismic zoning information in the newly proposed building code (NC 46:2013; see Data and Resources). This proposal is based on an upgrade of García (2007) in terms of UHS. The new building code is proposed for a 1642-year return period, delineating five different zone levels. The data are presented for two periods S_S (short periods) and S_l (long periods). It seems, from other information present in the proposal that these periods could be associated with $S_S = 0.2$ s and $S_l = 1.0$ s. A comparison with our results for those return periods in two zones—eastern Cuba (Santiago de Cuba region) and western Cuba (a zone that includes Havana)—shows that our results, in terms of spectral acceleration (g), including epistemic deviation, are between 20% and 50% less than in the proposal for the new seismic building code. It is noted that we do not have enough information on the proposed Cuban building code to make a more detailed comparison.

The quantitative and qualitative enhancement of the historical earthquake information should have first priority in the future; this will establish the basis for higher quality predictive computations and analysis in the future. Distinctly to this end is the expansion of the seismic network so that all new data acquired are analyzed for reliable hypocenter

parameters. If the current networks do not perform adequately, then future calculations will continue to suffer under poor quality data.

Data and Resources

In preparing the earthquake catalog, several online resources were searched. The U.S. Geological Survey (USGS) databases were searched from ftp://hazards.cr.usgs.gov (last accessed February 2014). The International Seismological Centre (ISC) databases were searched both from ftp://www.isc.ac.uk/pub and http://www.isc.ac.uk (last accessed February 2014). The Global Centroid Moment Tensor Project database was searched online (http://www.globalcmt.org/CMTsearch.html, last accessed February 2014).

The software SEISAN, used in data preparation, is freely downloadable from the University of Bergen ftp site (ftp://ftp.geo.uib.no/pub/seismo/SOFTWARE, last accessed January 2015). The software used for hazard calculations, CRISIS2014, was obtained directly from the authors. The maps were prepared with Generic Mapping Tool (GMT), v.4.5.8 (Wessel and Smith, 1998), which is free software (http://gmt.soest.hawaii.edu, last accessed November 2013). The gnuplot program, v.4.4 (Williams and Kelly, 2010) was used for Figure 9; this program is also free (http://sourceforge.net/projects/gnuplot, last accessed October 2015).

The major mapped faults of the region (USGS Open-File Report; http://pubs.usgs.gov/of/1997/ofr-97-470/OF97-470K/spatial/doc/faq/flt6bg_faq.html#what, last accessed June 2015) were used in preparation of the fault model.

Some materials (earthquake catalogs and GMPEs use recommendations) were consulted from the Global Earthquake Model (GEM) project (www.globalearthquakemodel.org, last accessed June 2015). The seismic zoning information in the newly proposed building code can be found in the unpublished NC 46:2013, Construcciones sismorresistentes, Requisitos básicos para el diseño y construcción, Nueva propuesta de norma, La Habana, 100 pp (in Spanish).

Acknowledgments

The present project could only be completed due to a grant from the Norwegian Ministry of Foreign Affairs (MFA) administrated by the Norwegian Directorate for Civil Protection (Direktoratet for Samfunnssikkerhet og Beredskap [DSB]). We thank two reviewers (one anonymous and D. Sleijko) for their considerate suggestions to improve the article. The authors also thank their home institutions NORSAR and CENAIS for support during the work.

References

Abrahamson, N. A., and W. J. Silva (2008). Abrahamson & Silva NGA ground motion relations for the geometric mean horizontal component of peak and spectral ground motion parameters, *Final Report Prepared for the Pacific Earthquake Engineering Research Center*, February 2008.

Alvarez, L. (1985). Seismicity of eastern Cuba, *Ph.D. Thesis*, Institute of Physics of the Earth, Academy of Sciences of the USSR, Institute of Geophysics and Astronomy, Cuban Academy of Sciences, 162 pp. (in Russian).

Alvarez, L., and V. I. Bune (1985a). Seismic shakeability of eastern Cuba, *Fizika Zemli* **1985,** no. 10, 3–12 (in Russian).

Alvarez, L., and V. I. Bune (1985b). A computer program for seismic hazard estimation, *Proc. of the 3rd International Symposium on the Analysis of Seismicity and on Seismic Risk*, Liblice Castle, Czechoslovakia, 17–22 June, 432–439.

Alvarez, L., and T. Chuy (1985). Isoseismal model for Greater Antilles, *Proc. of the 3rd International Symposium on the Analysis of Seismicity and on Seismic Risk*, Liblice Castle, Czechoslovakia, 17–22 June, 134–141.

Alvarez, L., T. Chuy, J. Garcia, B. Moreno, H. Alvarez, M. Blanco, O. Exposito, O. Gonzalez, and A. I. Fernandez (1999). An earthquake catalogue of Cuba and neighboring areas, *ICTP Internal Report IC/IR/99/1*, Miramare, Trieste, 60 pp.

Alvarez, L., R. S. Mijáilova, E. O. Vorobiova, T. J. Chuy, G. N. Zhakirdzhánova, E. R. Pérez, L. M. Rodiónova, H. Alvarez, and K. M. Mirzoev (2000). Terremotos de Cuba y áreas aledañas, *Sismicidad de Cuba y estructura de la corteza en el Caribe. La Habana, Editorial Academia*, 7–35, ISBN: 959-02-0242-X (in Spanish).

Arango, E. D. (1996). Geodinámica de la región de Santiago de Cuba en el límite de las placas de Norteamérica y el Caribe, *M.Sc. Thesis*, National Polytechnic Institute of Mexico. 110 pp. (in Spanish).

Ashish, C., Lindholm, I. A. Parvez, and D. Kuhn (2016). Probabilistic earthquake hazard assessment for Peninsular India, *J. Seismol.* **26,** no. 2, 629–653, doi: 10.1007/s10950-015-9548-2.

Atkinson, G. M., and D. M. Boore (2006). Earthquake ground-motion prediction equations for eastern North America, *Bull. Seismol. Soc. Am.* **96,** 2181–2205.

Benford, B., C. De Mets, and E. Calais (2012). GPS estimates of microplate motions, northern Caribbean: Evidence for a Hispaniola microplate and implications for earthquake hazard, *Geophys. J. Int.* **191,** 481–490.

Bormann, P., K. Fujita, K. G. Mackey, and A. Gusev (2012). The Russian K-class system, its relationships to magnitudes and its potential for future development and application, in *New Manual of Seismological Observatory Practice 2 (NMSOP-2)*, P. Bormann (Editor), Deutsches GeoForschungsZentrum GFZ, Postdam, Germany, 1–27, doi: 10.2312/GFZ.NMSOP-2_IS_3.7.

Calais, E., and B. de Lépinay (1991). From transtension to transpression along the northern Caribbean plate boundary off Cuba: Implications for the recent motion of the Caribbean plate, *Tectonophysics* **186,** 329–350.

Campbell, K., and Y. Bozorgnia (2008). NGA ground motion model for the geometric mean horizontal component of PGA, PGV, PGD and 5% damped linear elastic response spectra for periods ranging from 0.01 to 10 s, *Earthq. Spectra* **24,** 139–171.

Chuy, T., and L. Alvarez (1995). Mapa de peligrosidad sísmica de Cuba para la nueva norma sísmica de la República de Cuba, CENAIS, Archives of the Cuban National Center for Seismological Research (CENAIS), CITMA, 21 pp. (in Spanish).

Cotilla, M., and L. Alvarez (1991). Principios del mapa sismotectónico de Cuba, *Rev. Geofís.* **35,** 113–124 (in Spanish).

Crespo, M. J., F. Martínez, and J. Martí (2014). Seismic hazard of the Iberian Peninsula: Evaluation with kernel functions, *Nat. Hazards Earth Syst. Sci.* **14,** 1309–1323.

DeMets, C., and M. Wiggins-Grandison (2007). Deformation of Jamaica and motion of the Gonâve microplate from GPS and seismic data, *Geophys. J. Int.* **168,** 362–378.

DeMets, C., P. E. Jansma, G. S. Mattioli, T. Dixon, F. Farina, R. Bilham, E. Calais, and P. Mann (2000). GPS geodetic constraints on Caribbean–North America plate motion, *Geophys. Res. Lett.* **27,** 437–440.

Douglas, J., F. Cotton, N. A. Abrahamson, S. Akkar, D. M. Boore, and C. Di Alessandro (2013). Pre-selection of ground motion prediction equations, *Report Produced in Context of GEM GMPE Project, Version: 1.0.0.*, 77 pp., available at https://www.globalearthquakemodel.org/ (last accessed June 2015).

Engdahl, E. R., R. van der Hilst, and R. Buland (1998). Global teleseismic earthquake relocation with improved travel times and procedures for depth determination, *Bull. Seismol. Soc. Am.* **88,** 722–743.

Fedotov, S. A., and S. L. Shumilina (1971). Seismic hazard of Kamchatka, *Izv. Akad. Nauk S.S.S.R., Fizika Zemli* **9,** 3–15 (in Russian).

García, J. (2007). Estimados de peligrosidad sísmica con el error asociado para Cuba y cálculo de pérdidas para la ciudad de Santiago de Cuba usando técnicas SIG, *Ph.D. Thesis*, La Habana, CENAIS-IGA, 197 pp. (in Spanish).

García, J., D. Slejko, L. Alvarez, L. Peruzza, and A. Rebez (2003). Seismic hazard maps for Cuba and surrounding areas, *Bull. Seismol. Soc. Am.* **93,** 2563–2590.

Garcia, J., D. Slejko, A. Rebez, M. Santulin, and L. Alvarez (2008). Seismic hazard map for Cuba and adjacent areas using the spatially smoothed seismicity approach, *J. Earthq. Eng.* **12,** 173–196.

Gardner, J. K., and L. Knopoff (1974). Is the sequence of earthquakes in southern California, with aftershocks removed, Poissonian?, *Bull. Seismol. Soc. Am.* **64,** 1363–1367.

Iturralde-Vinent, M. (1998). Sinopsis de la Constitución Geológica de Cuba, *Acta Geol. Hisp.* **33,** 9–56 (in Spanish).

Iturralde-Vinent, M. (Editor) (1996). Ofiolitas y arcos volcánicos de Cuba, *First Contribution of IGCP Project 364 "Geological Correlation of Ophiolites and Volcanic Arc Terrains in the Circum Caribbean Region"*, Miami, Florida, 265 pp. (in Spanish).

Molina, S., C. D. Lindholm, and H. Bungum (2001). Probabilistic seismic hazard analysis: Zoning free versus zoning methodology, *Boll. Geofis. Teor. Appl.* **42,** 19–40.

Ordaz, M., O. D. Cardona, M. A. Salgado-Gálvez, G. A. Bernal-Granados, S. K. Singh, and D. Zuloaga-Romero (2014). Probabilistic seismic hazard assessment at global level, *Int J Disaster Risk Reduct.* **10,** 419–427.

Ornthammarath, T., C. G. Lai, A. Menon, M. Corigliano, G. R. Dodagoudar, and K. Gonavaram (2008). Seismic hazard at the historical site of Kancheepuram in southern India, *The 14th World Conf. on Earthquake Engineering*, Beijing, China, 12–17 October 2008.

Ottemöller, L., P. Voss, and J. Havskov (2013). *SEISAN earthquake analysis software for Windows, Solaris, Linux and MacOSX. Version 10.0*, 409 pp.

Pezeshk, S., A. Zandieh, and B. Tavakoli (2011). Hybrid empirical ground-motion prediction equations for eastern North America using NGA models and updated seismological parameters, *Bull. Seismol. Soc. Am.* **101,** 1859–1870.

Rautian, T. G., V. I. Khalturin, K. Fujita, K. G. Mackey, and A. D. Kendall (2007). Origins and methodology of the Russian energy K-class system and its relationship to magnitude scales, *Seismol. Res. Lett.* **78,** 579–590.

Rodríguez, M., and L. Alvarez (1996). *Estimaciones Probabilísticas de la Peligrosidad Sísmica en Cuba*, CENAIS-MAPFRE, 94 pp. (in Spanish).

Rodríguez, M., L. Alvarez, and J. Garcia (1997). Estimaciones probabilísticas de la peligrosidad sísmica en Cuba, *Rev. Geofís.* **47,** 46–77.

Rosencrantz, E., and P. Mann (1991). SeaMARC II mapping of transform faults in the Cayman trough, Caribbean Sea, *Geology* **19,** 690–693.

Rubio, M. (1985). The assessment of seismic hazard for the Republic of Cuba, *Proc. of the 3rd International Symposium on the Analysis of Seismicity and on Seismic Risk*, Liblice Castle, Czechoslovakia, 17–22 June, 424–431.

Scordilis, E. M. (2006). Empirical global relations converting M_s and m_b to moment magnitude, *J. Seismol.* **10,** 225–236.

Stepp, J. C. (1972). Analysis of completeness of the earthquake sample in the Puget Sound area and its effect on statistical estimates of earthquake hazard, *Proc. of First Int. Conf. on Microzonazion*, Vol. 2, Seattle, Washington, 897–910.

Storchak, D. A., D. Di Giacomo, I. Bondár, E. R. Engdahl, J. Harris, W. H. K. Lee, A. Villaseñor, and P. Bormann (2013). Public release of the ISC-GEM global instrumental earthquake catalogue (1900–2009), *Seismol. Res. Lett.* **84,** no. 5, 810–815, doi: 10.1785/0220130034.

Utsu, T. (1971). Aftershocks and earthquake statistic (III). Analysis of the distribution of earthquake in magnitude, time and space with special consideration to clustering characteristics of earthquake occurrence (1). *J. Fac. Sci., Hokkaido Univ., Ser. VII* **3,** no. 5, 379–441.

Wessel, P., and W. H. F. Smith (1998). New, improved version of Generic Mapping Tools released, *Eos Trans. AGU* **79,** no. 47, 579.

Williams, T., and C. Kelly (2010). *gnuplot 4.4, An Interactive Plotting Program, Manual*, 224 pp.

Woo, G. (1996). Kernel estimation methods for seismic hazard area source modeling, *Bull. Seismol. Soc. Am.* **86,** 353–362.

Centro Nacional de Investigaciones Sismológicas
Departamento de Sismología de La Habana
Calle 212 No. 2916 e/ 29 y 31
La Coronela, Habana 16600
Cuba
leoalvar@cenais.cu
(L.A.)

NORSAR
P.O. Box 53
NO-2027 Kjeller
Norway
conrad@norsar.no
(C.L.)

Centro Nacional de Investigaciones Sismológicas
Calle 17 No. 61 e/ 4 y 6
Reparto Vista Alegre
Santiago de Cuba 90400
Cuba
madelin@cenais.cu
(M.V.)

Manuscript received 7 March 2016